AGU PUBLICATIONS

Geophysical Research Letters

RESEARCH LETTER
10.1002/2017GL075643

Key Points:
- The mean meridional circulation in the lower thermosphere is difficult to observe but can be derived from trace species distribution
- Maximum vertical gradient of CO_2 at summer high latitudes shows vertical wind convergence of mesosphere and lower thermosphere circulations
- Maximum vertical gradient of CO_2 at winter high latitudes reflects vertical wind convergence of the two thermospheric circulations

Correspondence to:
L. Qian,
lqian@ucar.edu

Citation:
Qian, L., Burns, A. & Yue, J. (2017). Evidence of the lower thermospheric winter-to-summer circulation from SABER CO_2 observations. *Geophysical Research Letters*, *44*, 10,100–10,107. https://doi.org/10.1002/2017GL075643

Received 11 SEP 2017
Accepted 4 OCT 2017
Accepted article online 9 OCT 2017
Published online 18 OCT 2017

Evidence of the Lower Thermospheric Winter-to-Summer Circulation From SABER CO_2 Observations

Liying Qian[1], Alan Burns[1], and Jia Yue[2,3]

[1]High Altitude Observatory, National Center for Atmospheric Research, Boulder, CO, USA, [2]Center for Atmospheric Science, Hampton University, Hampton, VA, USA, [3]ESSIC, University of Maryland, College Park, MD, USA

Abstract Numerical studies have shown that there is a lower thermospheric winter-to-summer circulation that is driven by wave dissipation and that it plays a significant role in trace gas distributions in the mesosphere and lower thermosphere, and in the composition of the thermosphere. However, the characteristics of this circulation are poorly known. Direct observations of it are difficult, but it leaves clear signatures in tracer distributions. The Sounding of the Atmosphere using Broadband Emission Radiometry (SABER) onboard the Thermosphere Ionosphere Mesosphere Energetics and Dynamics satellite has obtained CO_2 concentration from 2002 to present. This data set, combined with simulations by the Whole Atmosphere Community Climate Model, provides an unprecedented opportunity to infer the morphology of this circulation in both the summer and winter hemispheres. Our study show that there exists a maximum vertical gradient of CO_2 at summer high latitudes, driven by the convergence of the upwelling of the mesospheric circulation and the downwelling of the lower thermospheric circulation; in the winter hemisphere, the maximum vertical gradient of CO_2 is located at a higher altitude, driven by the convergence of the upwelling of the lower thermospheric circulation and the downwelling of the solar-driven thermospheric circulation; the bottom of the lower thermospheric circulation is located between ~ 95 km and 100 km, and it has a vertical extent of ~10 km. Analysis of the SABER CO_2 and temperature at summer high latitudes showed that the bottom of this circulation is consistently higher than the mesopause height by ~10 km.

1. Introduction

Temperatures in the summer mesosphere are the coldest in the atmosphere. This unusual seasonal variation of temperature is driven by gravity wave breaking near the mesopause region, causing a zonal wind reversal near the mesopause, which, under the Coriolis effect, induces a mean meridional summer-to-winter circulation. This meridional circulation diverges in the summer hemisphere, causing upwelling, and converges in winter causing downwelling. The upwelling in the summer mesosphere thus causes a cold summer mesopause through adiabatic cooling, whereas the downwelling in the winter mesosphere causes a warm winter mesopause through adiabatic warming (e.g., Garcia & Solomon, 1985; Holton, 1983; Lindzen, 1981). The summer-to-winter meridional circulation in the mesosphere is often referred to as the mesospheric residual circulation (Andrews & McIntyre, 1976), to account for transport of tracers by the zonal-mean meridional circulation and eddies. In the mesosphere and lower thermosphere (MLT), the residual circulation can largely be represented by the zonal-mean meridional circulation, since the difference between the two is small.

In addition to the well-known mesospheric meridional circulation described above, numerical model simulations show that there exists a winter-to-summer mean meridional circulation in the lower thermosphere just above the mesospheric summer-to-winter circulation, in the altitude region of ~100 km–110 km (Liu, 2007; Smith et al., 2011). This meridional wind causes upwelling in the winter hemisphere and downwelling in the summer hemisphere. The lower thermospheric meridional wind is driven by gravity wave forcing that is in the opposite direction to the gravity wave forcing that drives the mesospheric meridional wind.

Figure 1 is a schematic of these two, opposite gravity wave forcing processes, in the northern hemisphere, for January and July. Figure 1 is based on Figure 3 of Lindzen (1981), but it extends Figure 3 of Lindzen (1981) to include an illustration of a spectrum of gravity waves. The green lines denote the background mean zonal winds in winter and summer. In either month, most of the waves with phase speed that is in the same direction as the mean flow are filtered out as they propagate upward (shaded regions in the gravity wave spectrum), whereas the waves with phase speed opposite to the mean flow reach the mesopause region and

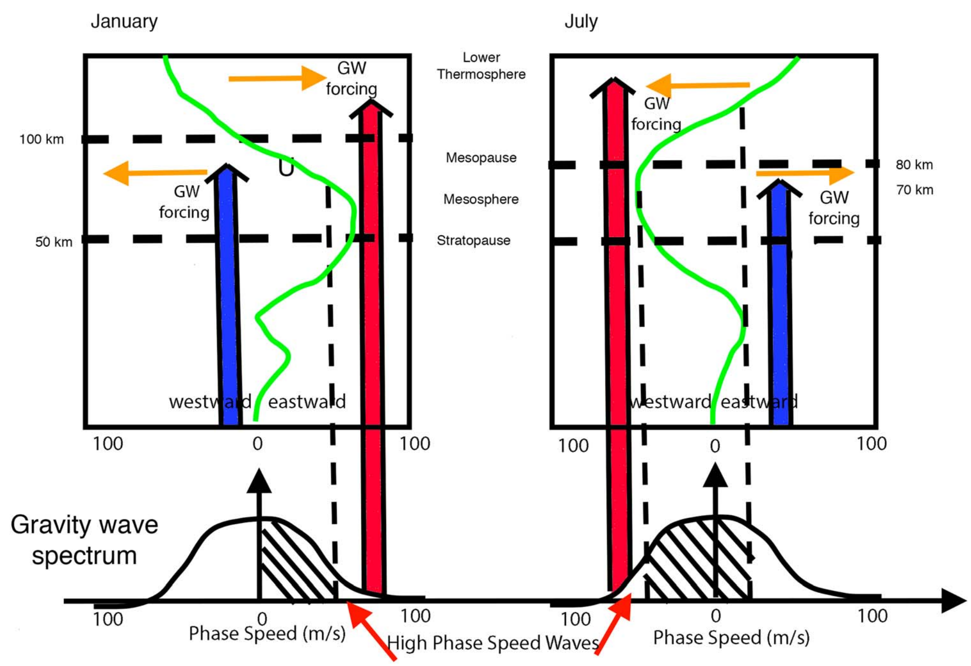

Figure 1. (top and bottom) Schematic of a spectrum of gravity waves, wave filtering, and wave momentum deposition in the MLT in the northern hemisphere. This schematic is based on Figure 3 of Lindzen (1981), but it extends Figure 3 of Lindzen (1981) to include an illustration of a spectrum of gravity waves. Left: January; right: July. The green lines are the background mean zonal winds. The shaded regions in the gravity wave spectrum indicate waves with phase speed that is in the same direction as the background mean zonal wind and thus are filtered as they propagate upward. The waves with phase speed that is in the opposite direction of the background mean zonal wind propagate into the mesopause region, break, and deposit their momentum there (blue columns). The high phase speed waves in the spectrum are indicated by the red arrows. These waves, although with phase speed that is in the same direction as the background mean zonal winds, propagate into the lower thermosphere due to their high phase speed, dissipate, and deposit momentum there (red columns). Gravity wave momentum deposition, which causes the background zonal wind reversal in the MLT region, is denoted by the orange arrows (left-pointing arrows: westward momentum deposition; right-pointing arrows: eastward momentum deposition).

break there (blue columns). This wave breaking causes zonal wind reversal by driving an eastward jet in summer and westward jet in winter (orange arrows; left-pointing arrows: westward momentum deposition; right-pointing arrows: eastward momentum deposition), which, under the Coriolis effect, drives a strong summer-to-winter meridional circulation. This gravity wave forcing drives the mesospheric meridional circulation. On the other hand, gravity waves with high phase speed (pointed to by the red arrows in the gravity wave spectrum), although in the same direction as the background mean zonal winds, can propagate into the lower thermosphere, dissipate there due to molecular diffusion and ion drag (red columns), and thus deposit momentum that is in the opposite direction to that which is deposited in the mesosphere (orange arrows; left-pointing arrows: westward momentum deposition; right-pointing arrows: eastward momentum deposition). Therefore, this momentum deposition drives westward zonal winds in summer and eastward zonal winds in winter, which, under the Coriolis effect, drives a winter-to-summer meridional wind (Liu, 2007).

Recent studies indicate that the lower thermospheric circulation is very important both for trace gas distributions in the MLT (e.g., Smith et al., 2011; Rezac, Jian, et al., 2015) and for thermospheric composition and its variability (Qian & Yue, 2017). However, there have been very few studies regarding this circulation. Our knowledge of the lower thermospheric circulations has so far come from numerical modeling studies (Liu, 2007; Smith et al., 2011; Rezac, Jian, et al., 2015). The generation and characteristics of the modeled lower thermospheric, meridional circulation are determined by the gravity wave parameterization scheme used. A gravity wave parameterization scheme assumes a spectrum of gravity waves, which has large uncertainty. On the other hand, winds in this altitude region are dominated by tides, with large-amplitude diurnal tides at low latitudes (e.g., Hagan & Forbes, 2002; Wu et al., 2008) and large-amplitude semidiurnal tides at midlatitudes (e.g., Hagan & Forbes, 2003). In addition, the mean meridional wind is considerably smaller than the amplitudes of these tides in the lower thermosphere. Therefore, the mean meridional wind in this region is difficult to measure. McLandress et al. (1996) illustrated the difficulty of making these observations when they analyzed horizontal winds in the altitude region of 50–200 km observed by the Wind Imaging Interferometer and the high-resolution Doppler imager onboard the Upper Atmosphere Research Satellite (UARS). They found that the meridional mean wind field between 90 and 120 km showed cell-like patterns, probably due to aliasing of temporally varying diurnal tides, which is a problem inherent in UARS data analysis since it took about 36 days to cover a full 24 h of local time at a given latitude.

Although the lower thermospheric, meridional circulation is difficult to directly observe and characterize, it leaves clear signatures in trace species distributions. Previous studies have examined distributions of CO_2 in this region (e.g., Kaufmann et al., 2002; López-Puertas et al., 2000), and wind effects on the CO_2 distribution are evident. For example, Kaufmann et al. (2002) analyzed CO_2 concentrations derived from the CO_2 emission band at 4.3 μm observed by the Cryogenic Infrared Spectrometers and Telescopes for the Atmosphere (CRISTA) aboard the Astronomical Shuttle Pallet Satellite, for the period of 8–15 August 1997. They found that in the northern hemisphere summer, below 90 km, CO_2 density increases toward high northern latitudes due to the mesospheric summer-to-winter meridional circulation; between 90 km and 120 km, downwelling that is dynamically linked to aurora conditions at summer high latitudes causes CO_2 volume mixing ratio (VMR) to decrease at the summer high latitudes, and thus reverses the latitudinal variation of CO_2 density. This morphology of the latitudinal distribution of CO_2 is evident in CO_2 VMR observed by the Sounding of the Atmosphere using Broadband Emission Radiometry (SABER) onboard the Thermosphere Ionosphere Mesosphere Energetics and Dynamics (TIMED) satellite (Rezac, Jian, et al., 2015).

Although previous studies have shown the importance of the lower thermospheric circulation in tracer distributions and thermospheric composition, and signatures of wind effects on CO_2 distributions, very little work has been undertaken to understand the characteristics of this circulation. The focus of this paper is thus to infer and understand the morphology of this lower thermospheric circulation, using TIMED/SABER data from 2002 to 2016, and simulations by the Specified Dynamics (SD) runs of the NCAR/WACCM (National Center for Atmospheric Research Whole Atmosphere Community Climate Model). SABER makes similar limb-scanning observations of CO_2 emission bands at 4.3 μm and 15 μm as those made by CRISTA but extends CRISTA observations on both spatial and seasonal coverage, as well as the span of the data sets. CRISTA-1 and CRISTA-2 each made observations for about 8 days, whereas SABER has measured CO_2 emissions from 2002 to present. This data set, combined with simulations by WACCM, provides an unprecedented opportunity that allowed us to infer and understand the characteristics of the lower thermospheric circulation in both the summer and winter hemispheres in this study, using more than 15 years of data. Section 2 gives a brief description of the data and model, section 3 presents results, and section 4 concludes our study.

2. Data and Model

2.1. TIMED/SABER CO_2 VMR and Temperature

SABER CO_2 will be used as a tracer to understand the lower thermospheric meridional circulation. The SABER temperature data will be used to understand the height of the lower thermospheric circulation in relation to the mesopause height. SABER is an instrument on board the TIMED satellite, which was launched on 7 December 2001 into a 74.1° inclination orbit at 630 km altitude. The SABER infrared sensors perform limb scans that provide simultaneous radiance profiles in 10 spectral channels over the range of 1.27–17 μm, with about 1400 profiles a day (Russell et al., 1999). The latitude coverage is 82°N–54°S or 54°N–82°S, with alternating coverage due to the spacecraft's 60 day yaw cycle. The SABER channels include CO_2 emission bands at 4.3 μm and 15 μm. A two-channel algorithm was used to simultaneously retrieve profiles of kinetic temperature T_k and CO_2 VMR from daytime radiance measurements, in the altitude range of 65–110 km (Rezac, Jian, et al., 2015, Rezac, Kutepov, et al., 2015). Detailed descriptions of the SABER instrument and data retrieval can be found in Russell et al. (1999), Remsberg et al. (2008), and Rezac, Kutepov, et al. (2015).

2.2. WACCM

SD-WACCM-simulated CO_2 VMRs are compared in this paper with the CO_2 VMR retrieved from the TIMED/SABER measurements. The corresponding meridional circulation patterns in the MLT region are

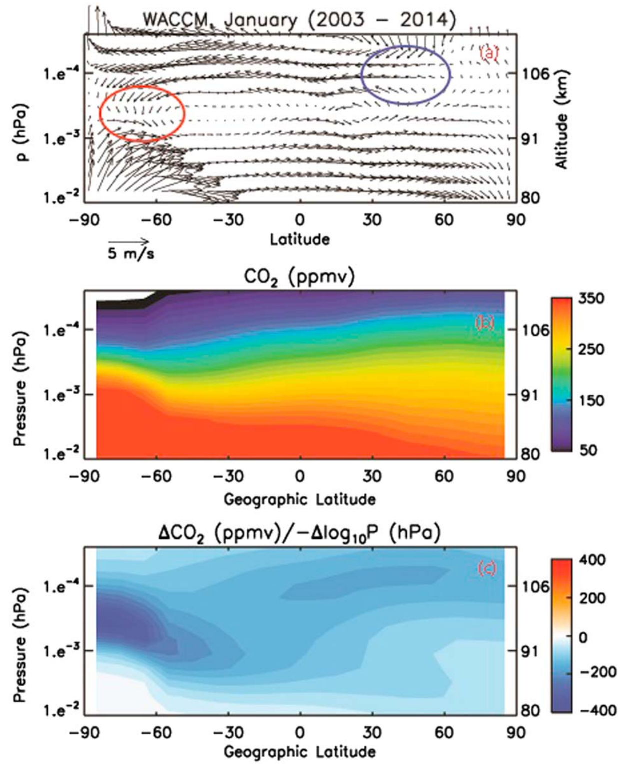

Figure 2. SD-WACCM mean fields (2003–2014) for January. (a) Residual meridional circulations, (b) CO_2, and (c) vertical gradient of CO_2. The vertical gradient was calculated as $\Delta CO_2/(-\Delta \log_{10} P)$.

used to interpret the CO_2 VMR morphology. WACCM is a global climate model with interactive chemistry. It covers the altitude range of 0–140 km. Existing SD-WACCM results from 2003 to 2014 will be used for this study. In these specified dynamics runs, WACCM v4 (Marsh et al., 2013) was constrained by Modern-Era Retrospective Analysis for Research and Applications (MERRA), which is a NASA reanalysis for the satellite era using a major new version of the Goddard Earth Observing System Data Assimilation System Version 5 (Rienecker et al., 2011); therefore, the dynamics in SD-WACCM-X will follow MERRA observations that contain realistic dynamic variability (below about 1 hPa (50 km)). The model transitions to free running above about 1 hPa (50 km) (Kunz et al., 2011).

3. Results

Figure 2a shows the mean residual circulations for January, calculated using output from SD-WACCM, for the period from 2003 to 2014. There are three circulation cells in Figure 2a: the summer-to-winter mesospheric circulation below ~95 km, with upwelling in summer and downwelling in winter, and the lower thermospheric winter-to-summer circulation between ~95 km and ~110 km, with upwelling in winter and downwelling in summer. Above ~110 km, it is the thermospheric solar-driven summer-to-winter circulation. Figure 2b shows the simulated CO_2 VMR. The source region of CO_2 is in the troposphere, and it is a nonreactive species in the lower and middle atmosphere; consequently, CO_2 is well mixed with a constant VMR from the source region to most part of the mesosphere due to turbulent mixing. It deviates from being well mixed as low as between ~70 km and 80 km (e.g., Kaufmann et al., 2002) due to molecular diffusion, horizontal and vertical wind advection, and photolysis above ~90 km. This height where a species with a long chemical lifetime starts to deviate from being well mixed is different for different species mainly due to their different molecular weight. In this paper, we refer to this height for CO_2 as the CO_2 homopause. On a global average basis, which largely averages out the wind advection effect, for a chemical species that has a long chemical lifetime compared to transport processes, such as CO_2 (Garcia et al., 2014), this height is primarily a balance between eddy diffusion and molecular diffusion. It is evident that the SD-WACCM-simulated CO_2 deviates from being well mixed at a lower altitude in winter than in summer (Figure 2b).

Since the source of CO_2 is in the lower atmosphere, upwelling increases local CO_2 above the well-mixed region, whereas downwelling decreases it in this region. Consequently, in summer, the convergence zone of the upwelling of the mesospheric circulation and the downwelling of the lower thermospheric circulation (red oval in Figure 2a) creates a zone with dense isolines (levels of constant CO_2 VMR) of CO_2 and thus forms a region with large vertical gradients of CO_2 at the summer high latitudes (Figure 2c). The vertical gradient is calculated as $\Delta CO_2/(-\Delta \log_{10} P)$, where the units of CO_2 and P are ppmv and hPa, respectively. This vertical gradient of CO_2 is negative when CO_2 VMR decreases with altitude. The height with the maximum vertical gradient of CO_2 indicates the transition altitude between the two circulation cells. This altitude is also the lower boundary of the lower thermospheric winter-to-summer circulation. Similarly, in the winter hemisphere, the convergence zone of the upwelling of the lower thermospheric circulation and the downwelling of the solar-driven thermospheric circulation (blue oval in Figure 2a) forms a region with large vertical gradients of CO_2 above 106 km (Figure 2c). The height of the maximum CO_2 gradient indicates the upper boundary of the lower thermospheric circulation. Figure 2a shows that the lower thermospheric circulation has a small vertical extent of ~10 km, from ~95 km to ~105 km.

It is important to note that the transition altitudes are different from the CO_2 homopause. The homopause is primarily determined by a balance between eddy diffusion and molecular diffusion on a global mean basis but is greatly impacted by the vertical advection locally. The CO_2 homopause observed by TIMED/SABER is

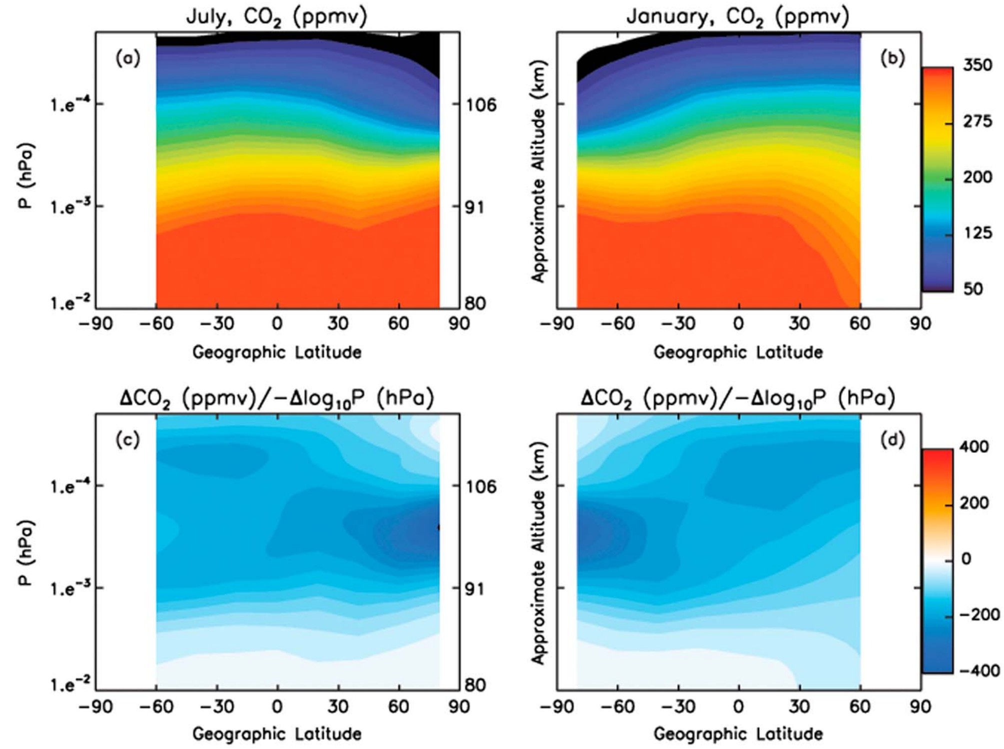

Figure 3. SABER CO_2 calculated January and July averages using data from 2003 to 2016, (a) July and (b) January, and the corresponding vertical gradients of CO_2. The vertical gradient was calculated as $\Delta CO_2/(-\Delta \log_{10} P)$. (c) July and (d) January.

below 90 km (Rezac, Jian, et al., 2015). The circulation transition altitudes addressed here are above the CO_2 homopause. Although eddy diffusion and molecular diffusion impact the CO_2 concentration in the transition region, the major driving force that forms the transition altitude is the convergence of vertical winds.

Figure 3 shows climatological CO_2 VMR measured by SABER for the period from 2003 to 2016, and the corresponding vertical gradient of CO_2. The data for 2002 are not included in the calculation since SABER CO_2 data start on day 32th of 2002. CO_2 VMRs were binned into 20° latitude bins and averaged for July (Figure 3a) and January (Figure 3b). In the mesopause region, the CO_2 distribution during the solstice seasons has the characteristics of dense isolines in summer due to vertical wind convergence but spread-out isolines in winter due to vertical wind divergence. It is important to note that so far SABER CO_2 has been retrieved for daytime only. Consequently, there are no data at the winter high latitudes (>54°) as shown in Figures 3a and 3b. However, the vertical gradient of CO_2 between 0° and 54° in the winter hemisphere shown in Figure 2c, from SD-WACCM results, demonstrates that with SABER CO_2 data between 0° and 54° in the winter hemisphere, the corresponding CO_2 vertical gradients in this latitude range will be able to give a very good indication as to where the top boundary of the lower thermospheric winter-to-summer circulation is located in the winter hemisphere. Therefore, SABER CO_2 data should give enough information on the lower thermospheric circulation in both the summer and winter hemispheres. The bottom plots of Figure 3 shows the corresponding vertical gradients of CO_2 for July (Figure 3c) and January (Figure 3d). It is evident that the vertical gradient of CO_2 is the largest in the summer high latitudes.

A comparison between Figures 3d and 2c, which is the northern hemisphere winter case, shows that the simulated and observed vertical gradients of CO_2 are consistent in the key morphology: in the summer hemisphere, there is a region ~95 km–100 km with large vertical gradients of CO_2, reflecting the convergence between the upwelling of the summer mesospheric circulation and the downwelling of the lower thermospheric circulation. The maximum vertical gradient of SABER CO_2 in the summer high-latitude region is at ~97 km (Figure 3d). From the summer hemisphere to the winter hemisphere, this altitude of the maximum vertical gradient of CO_2 moves toward higher altitudes in both SABER data and SD-WACCM simulation

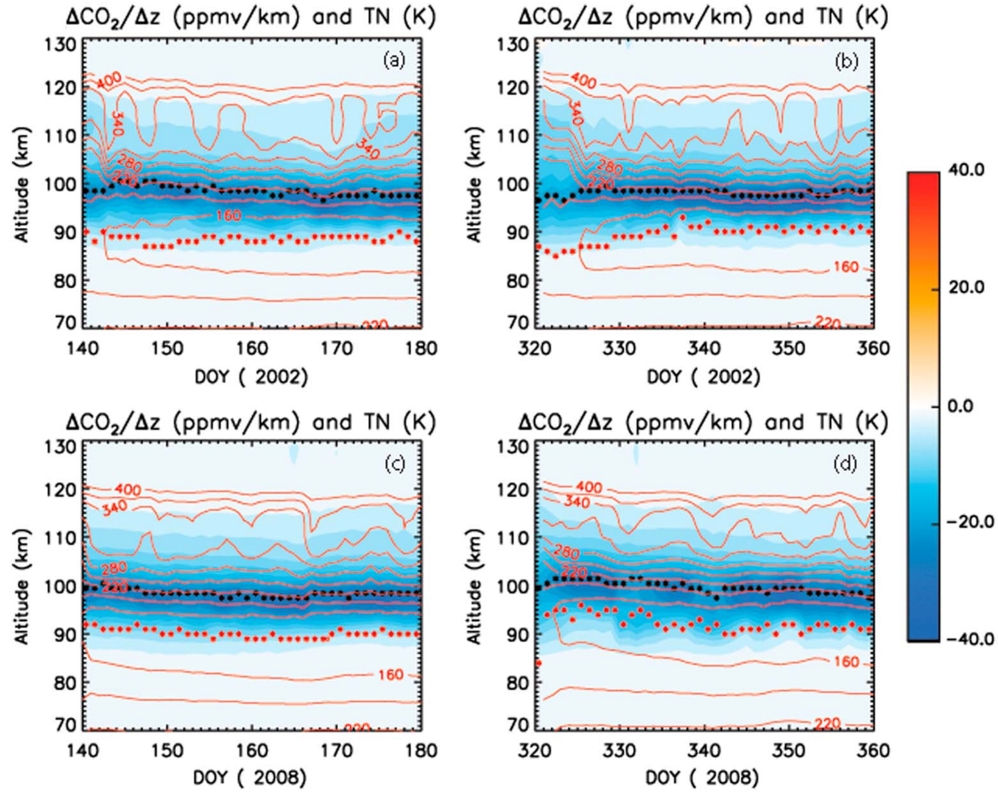

Figure 4. Daily average vertical gradients of SABER CO_2 VMR and SABER temperature at high latitudes (>50°) in the summer hemisphere. The vertical gradient is calculated as $\Delta CO_2/\Delta z$. The filled contours indicate vertical gradients of SABER CO_2; the red contour lines indicate SABER temperature. The black dotted lines show the bottom boundary of the lower thermospheric circulation; the red dotted lines show the mesopause height. (a) The northern hemisphere from day 140 to day 180 in 2002. (b) The southern hemisphere from day 320 to day 360 in 2002. (c) The northern hemisphere from day 140 to day 180 in 2008. (d) The southern hemisphere from day 320 to day 360 in 2008.

results, reflecting the convergence between the upwelling of the lower thermospheric circulation and the downwelling of the solar-driven thermospheric circulation. SABER data show that in the winter hemisphere the maximum vertical CO_2 gradient is at ~107 km at 60° latitude (Figure 3d). Therefore, SABER CO_2 data clearly show the signature of the lower thermospheric circulation as illustrated by the SD-WACCM simulation results shown in Figure 2.

We note that from the SABER CO_2 distribution, we can identify the bottom boundary of the lower thermospheric circulation in summer and the top boundary of the lower thermospheric circulation in winter, but we do not have direct information on the top boundary of this circulation in summer and the bottom boundary of this circulation in winter. However, based on the circulation patterns simulated by WACCM shown in Figure 2a, and the consistency between the simulated and observed vertical gradients of CO_2 (Figure 2c versus Figure 3d), we can infer that for January, the lower thermospheric circulation is between ~97 km and ~107 km, situated between the mesospheric circulation and the solar-driven thermospheric circulation. The lower thermospheric circulation for July is at a slightly lower altitude and with a smaller vertical extent compared to the January one (Figure 3).

It is of interest to know where the lower thermospheric circulation is located in relation to the mesopause height since the mesopause height is frequently used and commonly known, and since the mesospheric circulation cell affects both the temperature and height of the mesopause. The zonal wind reversal at the mesopause is stronger in the summer hemisphere, where the gravity wave forcing is larger than it is in the winter hemisphere. It occurs in a relatively narrow altitude range compared to the broader altitude range of the gravity wave forcing in the winter hemisphere (Liu, 2007; Smith et al., 2011). Similarly, the zonal wind reversal in the lower thermosphere is also stronger in the summer hemisphere (Liu, 2007). We note that the larger vertical gradients of CO_2 in the summer high-latitude regions are consistent with these stronger zonal wind reversals. Here we further investigated where the transition altitude from the mesospheric circulation cell to the lower thermospheric circulation cell is, in relation to the mesopause height in the summer hemisphere, using SABER temperature data.

Figure 4 shows daily average vertical gradients of SABER CO_2 VMR and SABER temperature at high latitudes ($>50°$) in the summer hemisphere, in a period of 40 days around the solstices, for the June solstice in 2002 (Figure 4a), the December solstice in 2002 (Figure 4b), the June solstice in 2008 (Figure 4c), and the December solstice in 2008 (Figure 4d). Note that since the mesopause height is an altitude, therefore, we calculated the vertical gradient of CO_2 VMR as $\Delta CO_2/\Delta z$, where z is altitude in kilometer. We calculated the vertical gradient of CO_2 VMR as $\Delta CO_2/(-\Delta \log_{10} P)$, for the purpose of model-data comparisons in Figures 2 and 3 since the model output is in pressure coordinates. Note that the magnitude of the vertical gradient of CO_2 calculated in log10 of pressure is, mathematically, larger than the magnitude of the vertical gradient of CO_2 calculated in altitude grid. It is evident that the bottom boundary of the lower thermospheric circulation (black dotted lines) is consistently higher than the mesopause height (red dotted lines), by about 10 km. The black and red dotted lines show the altitudes of the maximum vertical gradient of CO_2 and the minimum temperature, respectively. The bottom boundary of the lower thermospheric circulation does not change much from solar maximum to solar minimum, and during the 40 day period around the solstices, but it is slightly higher near the December solstice compared to the June solstice. There is some evidence that there is interannual variability in the southern summer, which is not apparent in the northern summer. We will investigate the interannual variability further in a future paper.

4. Conclusions

Previous studies have shown that the lower thermospheric circulation is important for trace gas distributions in the MLT and in the composition of the thermosphere, but the characteristics of this circulation are poorly known. Direct measurement of this circulation is difficult since the wind in the lower thermosphere is dominated by tides, and the mean meridional wind is much smaller than the amplitudes of these tides. However, this circulation leaves clear signatures in tracer distributions. Previous studies have examined CO_2 distribution, and wind effects on the CO_2 distribution are evident. However, very little work has been undertaken to understand the characteristics of the lower thermospheric circulation. The availability of the CO_2 VMR obtained from SABER observations from 2002 to present, and SD-WACCM simulations, provides us an unprecedented opportunity to use CO_2 distributions to understand the morphology of this circulation.We found the following:

1. Both SABER CO_2 and SD-WACCM simulated CO_2 show a region of large vertical gradients of CO_2 in the summer high latitudes, and the altitude of the maximum vertical gradient of CO_2 is ~95 km–100 km. SD-WACCM simulations show that this is caused by the vertical wind convergence of the upwelling of the mesospheric circulation and the downwelling of the lower thermospheric circulation in the summer high latitudes;
2. From the summer hemisphere to the winter hemisphere, this altitude of the maximum vertical gradient of CO_2 moves toward higher altitudes. SD-WACCM simulations show that in the winter hemisphere, the maximum vertical gradient of CO_2 is caused by the vertical wind convergence of the upwelling of the lower thermospheric circulation and the downwelling of the solar-driven thermospheric circulation;
3. SABER CO_2 clearly shows the evidence of the winter-to-summer lower thermospheric circulation that is located between the summer-to-winter mesospheric circulation and the solar-driven summer-to-winter thermospheric circulation, in an altitude region between ~97 km and ~107 km in January. It is at a slightly lower altitude region in July;
4. Based on analysis of the SABER CO_2 and temperatures at the summer high latitudes, the bottom boundary of the lower thermospheric circulation is consistently higher than the mesopause height, by ~10 km. The bottom boundary of this circulation does not change much between solar maximum and solar minimum, it is slightly higher near the December solstice compared to the June solstice, and there is some evidence of interannual variability in the southern summer, which is not apparent in the northern summer.

Our understanding of the lower thermospheric circulation will be greatly improved when there are observations of other trace gases (e.g., O_2 and CO) in the MLT region and direct measurements of neutral winds in the region in the future. .

Acknowledgments
This research was supported by NASA grants NNH15ZDA001N-HSR, NNX13AE20G, NNX14AE06G, NNX15AB83G, and NNX14AC13G, to the National Center for Atmospheric Research. NCAR is sponsored by the National Science Foundation. We would like to thank the SABER team for the CO_2 measurements. SABER is supported by NASA grant NNX12AG45G. SABER version 2.0 data from 2002 to 2017 are available at ftp://saber.gats-inc.com/Version2_0/Level2C/. All model simulation results that produced the results in this paper are available on NCAR's High Performance Storage System upon request.

References

Andrews, D. G., & McIntyre, M. E. (1976). Planetary waves in horizontal and vertical shear: The generalized Eliassen-Palm relation and mean zonal acceleration. *Journal of the Atmospheric Sciences*, *33*, 2031–2048.

Garcia, R. R., López-Puertas, M., Funke, B., Marsh, D. R., Kinnison, D. E., Smith, A. K., & González-Galindo, F. (2014). On the distribution of CO_2 and CO in the mesosphere and lower thermosphere. *Journal of Geophysical Research: Atmospheres*, *119*, 5700–5718. https://doi.org/10.1002/2013JD021208

Garcia, R. R., & Solomon, S. (1985). The effect of breaking gravity waves on the dynamics and chemical composition of the mesosphere and lower thermosphere. *Journal of Geophysical Research*, *90*, 3850–3868. https://doi.org/10.1029/JD090iD02p03850

Hagan, M. E., & Forbes, J. M. (2002). Migrating and nonmigrating diurnal tides in the middle and upper atmosphere excited by tropospheric latent heat release. *Journal of Geophysical Research*, *107*(D24), 4754. https://doi.org/10.1029/2001JD001236

Hagan, M. E., & Forbes, J. M. (2003). Migrating and nonmigrating semidiurnal tides in the upper atmosphere excited by tropospheric latent heat release. *Journal of Geophysical Research*, *108*(A2), 1062. https://doi.org/10.1029/2002JA009466

Holton, J. R. (1983). The influence of gravity wave breaking on the general circulation of the middle atmosphere. *Journal of the Atmospheric Sciences*, *40*, 2497–2507.

Kaufmann, M., Gusev, O. A., Grossmann, K. U., Roble, R. G., Hagan, M. E., Hartsough, C., & Kutepov, A. A. (2002). The vertical and horizontal distribution of CO_2 densities in the upper mesosphere and lower thermosphere as measured by CRISTA. *Journal of Geophysical Research*, *107*(D23), 8182. https://doi.org/10.1029/2001JD000704

Kunz, A., Pan, L. L., Konopka, P., Kinnison, D. E., & Tilmes, S. (2011). Chemical and dynamical discontinuity at the extratropical tropopause based on START08 and WACCM analysis. *Journal of Geophysical Research*, *116*, D24302. https://doi.org/10.1029/2011JD016686

Lindzen, R. S. (1981). Turbulence and stress owing to gravity wave and tidal breakdown. *Journal of Geophysical Research*, *86*(C10), 9707–9714. https://doi.org/10.1029/JC086iC10p09707

Liu, H.-L. (2007). On the large wind shear and fast meridional transport above the mesopause. *Geophysical Research Letters*, *34*, L08815. https://doi.org/10.1029/2006GL028789

López-Puertas, M., López-Valverde, M. Á., Garcia, R. R., & Roble, R. G. (2000). *A review of CO_2 and CO abundances in the middle atmosphere*, *geophysical monograph* (Vol. 123, pp. 83–100). Washington, DC: American Geophysical Union.

Marsh, D. R., Mills, M. E., Kinnison, D. E., Lamarque, J.-F., Calvo, N., & Polvani, L. M. (2013). Climate change from 1850 to 2005 simulated in CESM1 (WACCM). *Journal of Climate*, *26*, 7372–7391. https://doi.org/10.1175/JCLI-D-12-0558.1

McLandress, C. M., Shepherd, G. G., Solheim, B. H., Burrage, M. D., Hays, P. B., & Skinner, W. R. (1996). Combined mesosphere/thermosphere winds using WINDII and HRDI data from the Upper Atmosphere Research Satellite. *Journal of Geophysical Research*, *101*, 10,441–10,453. https://doi.org/10.1029/95JD01706

Qian, L., & Yue, J. (2017). Impact of the lower thermospheric winter-to-summer residual circulation on thermospheric composition. *Geophysical Research Letters*, *44*, 3971–3979. https://doi.org/10.1002/2017GL073361

Remsberg, E. E., Marshall, B. T., Garcia-Comas, M., Krueger, D., Lingenfelser, G. S., Martin-Torres, J., … Thompson, R. E. (2008). Assessment of the quality of the version 1.07 temperature-versus pressure profiles of the middle atmosphere from TIMED/SABER. *Journal of Geophysical Research*, *113*, D17101. https://doi.org/10.1029/2008JD010013

Rezac, L., Jian, Y., Yue, J., Russell, J. M. III, Kutepov, A., Garcia, R., … Bernath, P. (2015). Validation of the global distribution of CO_2 volume mixing ratio in the mesosphere and lower thermosphere from SABER. *Journal of Geophysical Research: Atmospheres*, *120*, 12,067–12,081. https://doi.org/10.1002/2015JD023955

Rezac, L., Kutepov, A., Russell, J. M. III, Feofilov, A. G., Yue, J., & Goldberg, R. A. (2015). Simultaneous retrieval of T(p) and CO_2 VMR from non-LTE limb radiances measured by the SABER/TIMED instrument. *Journal of Atmospheric and Solar - Terrestrial Physics*, *130-131*, 23–42. https://doi.org/10.1016/j.jastp.2015.05.004

Rienecker, M. M., Suarez, M. J., Gelaro, R., Todling, R., Bacmeister, J., Liu, E., … Woollen, J. (2011). MERRA: NASA's Modern-Era Retrospective Analysis for Re-search and Applications. *Journal of Climate*, *24*, 3624–3648. https://doi.org/10.1175/JCLI-D-11-00015.1

Russell, J. M., III, Mlynczak, M. G., Gordley, L. L., Tansock, J., & Esplin, R. (1999). An over-view of the SABER experiment and preliminary calibration results, proceedings of the SPIE, 44th annual meeting, Denver, Colorado, July 18–23, 3756, 277–288.

Smith, A. K., Garcia, R. R., Marsh, D. R., & Richter, J. H. (2011). WACCM simulations of the mean circulation and trace species transport in the winter mesosphere. *Journal of Geophysical Research*, *116*, D20115. https://doi.org/10.1029/2011JD016083

Wu, Q., Ortland, D. A., Killeen, T. L., Roble, R. G., Hagan, M. E., Liu, H.-L., … Niciejewski, R. J. (2008). Global distribution and interannual variations of mesospheric and lower thermospheric neutral wind diurnal tide: 1. Migrating tide. *Journal of Geophysical Research*, *113*, A05308. https://doi.org/10.1029/2007JA012542